Targeting BTN2A1 enhances Vγ9Vδ2 T-cell effector functions and triggers tumor cell pyroptosis

Anne-Charlotte Le Floch, Caroline Imbert, Nicolas Boucherit, Laurent Gorvel, Stéphane Fattori, Florence Orlanducci, Aude Le Roy, Lorenzo Archetti, Lydie Crescence, Laurence Panicot-Dubois, et al.

Targeting BTN2A1 enhances Vγ9Vδ2 T-cell effector functions and triggers tumor cell pyroptosis

Anne Charlotte le Floch[1*], Caroline Imbert[1*], Nicolas Boucherit[1], Laurent Gorvel[1], Stéphane Fattori[1], Florence Orlanducci[1], Aude Le Roy[1], Lorenzo Archetti[2], Lydie Crescence[3], Laurence Panicot-Dubois[3], Christophe Dubois[3], Norbert Vey[4,5], Antoine Briantais[1], Amandine Anastasio[1], Carla Cano[6], Geoffrey Guittard[1], Mathieu Frechin[2], Daniel Olive[1,4,5†]

[1]Centre de Recherche en Cancérologie de Marseille, Inserm U1068, CNRS UMR7258, Aix Marseille Université U105, Institut Paoli Calmettes, 27 Boulevard Lei Roure CS30059, 13273 Marseille Cedex 09, France.

[2]Nanolive SA, Lake Geneva Park, Switzerland

[3]Aix-Marseille Université, INSERM 1263, INRA 1260, Center for Cardiovascular and Nutrition Research (C2VN), Marseille France

[4]Institut Paoli-Calmettes, 13009 Marseille, France;

[5]Aix-Marseille Université UM105, CNRS UMR 7258, 13009 Marseille, France

[6]ImCheck Therapeutics, 13009 Marseille, France;

* *These authors contributed equally*

[†] Corresponding author. Email : Daniel.Olive@inserm.fr, Phone: +33 (0) 486 977 271

Running title: BTN2A1 modulates γδ T-cell function and pyroptosis

Funding information: The authors thank the IPC Immunomonitoring platform and IPC Tumor Bank (authorization number AC-2007-33, granted by the French Ministry of Research. The “Immunity and Cancer” team was labeled “FRM DEQ20180339209” (D.O.). This work was supported by Imcheck Therapeutics and by the Institut National Du Cancer (grant 2012-064/2019-038; D.O.), the Sites de Recherche Intégrée sur le Cancer of Marseille (grant INCa-DGOS-INSERM 6038), the Association Laurette Fugain (grant ALF2020/05; D.O.), and the Agence Nationale de la Recherche (French National Infrastructure for Mouse Phenogenomics [PHENOMIN] project). A.-C.L.F. was funded by a Poste d’Accueil INSERM grant from November 2019 to October 2021.

Competing interests: D.O. is cofounder and shareholder of Imcheck Therapeutics. C.E.C is employee and shareholder of Imcheck Therapeutics. L.A. and M.F. are employees of Nanolive SA. The remaining authors declare no competing interests

Abstract

Vγ9Vδ2 T cells are potent but elusive cytotoxic effectors. Butyrophilin subfamily 2 member A1 (BTN2A1) is a surface protein that has recently been shown to bind the Vγ9 chain of the γδ T-cell receptor (TCR) but its precise role in modulating Vγ9Vδ2 T-cell functions remains unknown. Here, we show that 107G3B5, a monoclonal BTN2A1 agonist antibody, was able to significantly enhance Vγ9Vδ2 T-cell functions against hematological or solid cell lines and against primary cells from adult acute lymphoblastic leukemia patients. New computer vision strategies applied to holotomographic microscopy videos showed that 107G3B5 enhanced the interaction between Vγ9Vδ2 T cells and target cells in a quantitative and qualitative manner. In addition, we found that Vγ9Vδ2 T cells activated by 107G3B5 induced caspase 3/7 activation in tumor cells, thereby triggering tumor cell death by pyroptosis. Together, these data demonstrate that targeting BTN2A1 with 107G3B5 enhances the Vγ9Vδ2 T-cell antitumor response by triggering the pyroptosis-induced immunogenic cell death. These new pyroptosis-based therapies have great potential to stimulate the immune system to fight cancer, especially “cold” tumors.

Synopsis

Harnessing Vγ9Vδ2 T cells for cancer immunotherapy is of interest. The authors show that an agonist antibody targeting BTN2A1 sensitizes ALL and solid tumor models to Vγ9Vδ2 T cells, which can mobilize gasdermin E to induce tumor-cell pyroptosis.

Introduction

In contrast to activation of αβ T cells, γδ T-cell activation is MHC-unrestricted and relies on the detection of various host cell-derived molecules(1) or exogenous pathogens by both T-cell receptor (TCR) and non-TCR receptors. γδ T cells represent the earliest source of IFNγ secretion in the tumor microenvironment(2) and recent transcriptome analyses of human tumors have revealed that high γδ T-cell infiltration has the best prognostic value in comparison to other immune subsets(3,4). Vγ9Vδ2 T cells are the major subtype of blood γδ T cells and are activated by non-peptidic phosphorylated metabolites, called phosphoantigens (pAgs), produced by transformed or infected cells(5,6)

A better understanding of the mechanisms of action of Vγ9Vδ2 T cells will lead to new potential immunotherapies. In this context, the interaction between butyrophilin subfamily 3 member A (BTN3A) and BTN2A1 at the plasma membrane, which enables the recognition of pAgs by Vγ9Vδ2 T cells through an "inside-outside signaling" (7–9), is of particular interest. BTN3A1 cooperates with BTN2A1 for cell surface export and binds to pAgs through its intracellular B30.2 domain, which also stabilizes its interaction with BTN2A1 (10,11). After decades without a known ligand for the Vδ2 or Vγ9 chains, BTN2A1 was recently identified as a direct ligand for the Vγ9 chain of the γδ TCR (12,13), representing a fundamental new paradigm in Vγ9Vδ2 T-cell biology. While it is clear that BTN2A1 is mandatory for Vγ9Vδ2 T-cell activation in tumoral contexts(9,12,13), its precise role in modulating the functions of Vγ9Vδ2 T cells needs to be carefully investigated.

Vγ9Vδ2 T cells have been demonstrated to have antitumor activity in preclinical models(14–22), which led to clinical trials that predominantly evaluated pharmacological inducers of pAgs, such as aminobisphosphonates(23). While these clinical trials tended to show objective responses, they were associated with limited efficacy (24). So far, only one monoclonal antibody (mAb) targeting BTN3A molecules with the aim of modulating Vγ9Vδ2 T cells has reached clinical trials; it is currently being tested in the multicenter phase 1/2 EVICTION trial (25). In this study we describe a new mAb

targeting BTN2A to activate Vγ9Vδ2 T cells, which we hope could eventually provide new options for the treatment of patients with cancer.

Low tumor immunogenicity and a cold tumor microenvironment are two of the main features associated with resistance to immunotherapy. One possibility is to transform 'cold' tumors into 'hot' tumors by inducing immunogenic tumor cell death (26). Natural killer (NK) cells and cytotoxic T cells were traditionally thought to induce tumor cell death mainly by non-inflammatory apoptosis; however, several studies have recently revealed that these cells can suppress tumors by inducing immunogenic forms of cell death, including pyroptosis (27,28). Thus, activation of caspase 3/7 can lead to apoptosis, a non-inflammatory form of programmed cell death or pyroptosis, a pro-inflammatory form of cell death(29). The induction of non-apoptotic forms of cell death has attracted much attention in the field of antitumor therapy, but to our knowledge, until now, the ability of Vγ9Vδ2 T cells to induce pyroptosis or other forms of immunogenic cell death remained unknown.

Here, we show that a unique agonist mAb 107G3B5, which targets BTN2A1, enhances the cytotoxic activity of Vγ9Vδ2 T cells. We used several *in vitro* tumor models, including acute lymphoblastic leukemia (ALL) in both allogeneic and autologous settings, as well as solid tumor models. Newly developed computer vision powered by Artificial Intelligence (AI) was used to analyze videos recorded with label-free holotomographic microscopy, uncovering that 107G3B5 increased the quantity and quality of Vγ9Vδ2 T-cell interactions with target cells. These cellular events were associated with a clustering of BTN2A1 and its colocalization with BTN3A1, as demonstrated by confocal microscopy and fluorescence resonance energy transfer (FRET) experiments. Finally, we demonstrated that activation of Vγ9Vδ2 T cells using 107G3B7 induced tumor cell pyroptosis.

Material and methods

Patients and healthy volunteers

PBMCs from 28 adult ALL patients at diagnosis (10 B-ALL, 9 T-ALL and 9 Ph^+ ALL) were analyzed for their BTN expression level, and some were also tested in functional assays (7 B-ALL, 7 T-ALL and 3 Ph^+

ALL). Mean PB blasts of ALL samples was 84.3 (9.6), and these samples were therefore used as PB blasts without the need for an isolation in functional experiments. Heparinized blood from the ALL patients was obtained from the Hematology Department of the Institut Paoli Calmettes. ALL samples were stored in nitrogen. PBMCs from healthy volunteers (HV) were provided by the local Blood Bank (French Blood Establishment). Written informed consent was obtained from ALL patients and HV, in accordance with the Declaration of Helsinki, and the study was approved by the Institutional Review Board of the Institut Paoli Calmettes (BTN-LAL-IPC2021-049 - Immunomodulation dans les leucémies aigues - June 22, 2021). Baseline characteristics of ALL patients are provided in Table 1.

Cell lines

Cell lines derived from ALL (697, SUP-T1), anaplastic large-cell lymphoma (KARPAS-299), non-Hodgkin lymphoma (DAUDI), colorectal cancer (HT-29), prostate cancer (PC-3), cervical carcinoma (Caski) and endometrial cancer (Ishikawa) were obtained from the American Type Culture Collection or from DSMZ. In addition, we used HEK293T for microscopy experiments and binding assays. Cell line authentication was performed by the American Type Culture Collection (ATCC) based on criteria established by the International Cell Line Authentication Committee. Short tandem repeat profiling revealed that these cell lines were all above the 80% match threshold.

697 cells (DZMZ 2020, [1-2] passages) were cultured in RPMI 1640 with 20% Fetal Bovine Serum (FBS). HEK293T (ATCC 2019, [10-15] passages) were cultured in DMEM with 10% FBS. PC-3 (ATCC 2016, [10-15] passages), CaSki (ATCC 2020, [5-10] passages) and Ishikawa (ATCC 2018, [8-12] passages) were cultured in DMEM with 20% FBS. SUP-T1 (DSMZ 2012, [15-20] passages), KARPAS-299 (ATCC 2016, [20-25] passages), DAUDI (ATCC 2018, [15-20] passages) and HT-29 (ATCC 2018, [8-12] passages) were cultured in RPMI 1640 with 10% FBS. Generation of BTN3AKO/BTN2AKO HEK293T cells using CRISPR-Cas9-mediated inactivation of BTN2A and/or BTN3A was performed as previously described (9). The guide sequences used were the following: BTN3A, TTTCTGTGCTTGGACCCTCT; BTN2A, ACAGTGTGGAGGGACCCCTA. For the KARPAS-299 BTN2A1 knockout cell line the gRNA

TCACAAAGGTGGTTCTTCCT was cloned into plenti-CRISPR v2 plasmid and sequence-verified by Genscript. This plasmid or empty vector (for control cells) was used to transfect HEK293T cells using PEI max reagent (Thermo Fisher Scientific) in OptiMEM™ medium, according to the manufacturer's instructions. Culture supernatant containing lentiviral particles was collected after 48h. KARPAS-299 were seed in 24-wells plates (2,5x105 cells/well) and 200ul of lentiviral particules were add to culture. After 24 hours, cells were washed twice in complete medium and cultured in their regular medium. Three days after 1ug/ml of puromycin was added to culture medium for selection. The absence of BTN2A and/or BTN3A was confirmed by flow cytometry. All cell lines tested negative for mycoplasma using the MycoAlert Mycoplasme detection Kit (Lonza).

Expansion of Vγ9Vδ2 T cells

PBMCs from ALL patients and HV were isolated by density gradient (Lymphoprep). For ALL patients, cells were frozen until use. For establishment of allogenic Vγ9Vδ2 T cells, fresh PBMCs from 8 HV were cultured in RPMI 1640 (Gibco™) and stimulated with 1µM zoledronate (ZOL) (Sigma-Aldrich), and recombinant human IL2 (rhIl-2, 200 U/ml) (Miltenyi) at day 0. From day 5, rhIL-2 was renewed every two days and cells were kept at $1.5x10^6$/ml for 14 days. Only cell cultures that reached more than 80% of Vγ9Vδ2 T cells purity at day 14 were selected and frozen until use. The purity was analyzed by flow cytometry using Live/Dead (Invitrogen), anti-CD3 (BD Biosciences) and anti-TCR Vδ2 (Biolegend) markers. Allogeneic Vγ9Vδ2T-cells were thawed and cultured overnight in rhIL-2 (200 UI/mL) for use in functional assays.

For the establishment of autologous Vγ9Vδ2 T cells, frozen PBMCs from ALL patients were treated similarly but rhIL-15 (Miltenyi, 10ng/mL) was also added because it has been shown to increase their proliferative capacity(30–32). Fresh autologous expanded cells were then used for functional assays, depending on the quantity of Vγ9Vδ2 T cells. Fold increases of viable Vγ9Vδ2 T cells were calculated according to the formula: (%Vγ9Vδ2 at day 14 × total cell number at day 14)/ (% Vγ9Vδ2 at day 0 × total cell number at day 0).

Generation of anti-human BTN3A and BTN2A (clone7.48) mAbs

To generate anti-BTN3A 20.1 and anti-BTN3A 108.5 mAbs, BALB/c mice were immunized with a soluble BT3.1-Ig fusion protein, as previously described (33). Anti-BTN2A mAbs were produced by mouse immunization using a recombinant human BTN2A1-Fc fusion protein (R&D Biotech), as described in patent WO2019057933A1 (clone 7.48).

Identification of anti-BTN2A1 mAb 107G3B5

Mouse anti-human BTN2A1 were generated by immunizing 48 mice, bearing 6 different MHC combinations, with recombinant human BTN2A1-Fc (Biotechne) fusion protein. Mice were bled after 21 days and serum titer of BTN2A1-specific polyclonal antibodies was determined via Luminex assay. Mice displaying the highest BTN2A1-specific antibodies titer were euthanized. Splenic B cells were isolated via positive selection and underwent PEG-induced fusion to myeloma cells for hybridoma generation. Hybridomas were cloned by limiting dilution and hybridoma supernatants underwent two rounds of screening for target specificity and their capacity to induce degranulation of Vγ9Vδ2 T cells, and lead to the identification of 107G3B5.

Octet-based BTN2A1 affinity measurement:

After generation of anti-BTN2A1 107G3B5 in chimeric IgG1 format, affinities for the 2 different isoforms of this target (BTN2A1 and BTN2A2) were evaluated. Affinity and binning experiments were performed on an Octet Red96 platform (Fortebio/PALL), system based on Bio-layer interferometry (BLI) technology. For affinity experiments, recombinant human (rh)BTN2A1-Fc (GTP) was biotinylated using EZ-Link™ NHS-PEG4 Biotinylation Kit according to manufacturer's instructions, and biotinylated rhBTN2A2-Fc was purchased from R&D Systems. In the case of BTN2A1 affinity assays, biotinylated rhBTN2A1-Fc was loaded into streptavidin (SA) biosensors (ForteBio) diluted in Kinetic Buffer 1X (ForteBio) with a loading target level of around 1 nm, and chimeric anti-BTN2A antibodies were used

as analytes. For BTN2A2 affinity assays, 107G3B5 was loaded into FAB2G sensors (anti human CH1; Fortebio) as described above, and biotinylated rhBTN2A2-Fc was used as analyte. In both cases, analytes remained in solution and their working concentrations were diluted in Kinetic Buffer 10X (ForteBio). For the first run, the standard working concentration ranged from 200 to 3.125 nM. When necessary for the second run, working concentrations were adjusted from 80 to 1.25 nM. All runs (including loading, equilibration, association/dipping of sensors into analyte, dissociation and regeneration) were performed at 30°C with shaking 1000 rpm. Analysis was performed using a 1:1 or 2:1 Langmuir model (for BTN2A1 or BTN2A2, respectively) calculated by Octet software, which allowed a better fitting calculation.

Live-cell imaging of effector and target cell interactions

The target cells (T)— HEK293T, Ishikawa and SUP-T1 —were cultured overnight, or 1h for SUP-T1, on dishes (Ibidi, Gräfelfing, Germany) precoated with poly-L-lysine (respectively 0.5, 0.5, and 1 million cells). Non-adherent cells were removed by washing with PBS. Vγ9Vδ2 T cells expanded from healthy volunteers were added to the target cells (E:T ratio = 2:1 for HEK293T and SUPT-1, 3:1 for Ishikawa) in 1 ml of RMPI with 10% FBS. Isotype control antibody mouse IgG1 (Miltenyi) or BTN2A1-specific antibody 107G3B5 was added to the final concentration of 10 µg/mL. Dishes were incubated at 37°C with 5% CO_2 within Tokaihit stage top incubator (Ibidi) throughout the acquisitions, which were performed with a CX-A automated microscope A (Nanolive SA, Lake Geneva Park, Switzerland). The CX-A consists of an holotomographic microscope coupled to an automated stage that allows grid scanning and multi-well acquisition. The microscope uses a 60X air objective (NA = 0.8) at a wavelength of λ = 520 nm (Class 1 low power laser, sample exposure 0.2 mW/mm^2) and USB 3.0 CMOS Sony IMX174 sensor, single field of view 90 × 90 × 30 µm, axial resolution 400 nm, and maximum temporal resolution of 0.5 3D RI volume per second. The theoretical sensitivity of the refractive index (RI) measurement was 2.71×10^{-4}. The time lapse acquisition regime was one image every 9 minutes for 20 hours and was the same for all imaging experiments. The dynamics of the

lethal fraction were realized as previously described (34), using machine learning-based dead cell identification. The lethal fraction allows for the estimation of cell death in cases where the simple fraction of dead cells does not correctly represent the observed cell death throughout the experiment. This is the case when dead cells stop being visible during the acquisition, for example when they detach and exit from the field-of-view or are covered by living cells during time lapse experiments. Lethal fraction is calculated as follows:

$$LF = 1 - \frac{N_{living_{t=n}}}{\max\left(N_{dead_{t=o \rightarrow t=n}}\right) + N_{living_{t=n}}}$$

It can also be parametrized with a 5-parameter logistic curve to allow cell death kinetics calculations (e.g., cell death rate and maximum lethal fraction).

Quantification of effector–target cell interactions

Quantification of effector–/target cell interactions were performed using a software called the live T-Cell Assay developed and provided by Nanolive (https://www.nanolive.ch/products/live-cell-analytics/live-t-cell-assay/). This analysis consists of two steps, 1. detecting each cell object and its type, effector cells on one side, target cells on the other, based on their difference in size, morphology and texture, and then 2. quantifying the dynamic interactions between the two populations of cells. Four parameters were calculated and exploited in this study: the ratio of γδ T cells in contact with target cells, the average minimum distance between γδ T cells and target cell centroids, the percentage of target cell area covered by γδ T cells and the global movement speed of γδ T cells in µm/sec.

Transcriptomic expression of *BTN2A* and *BTN3A1*

Bulk RNA-seq of human normal or tumor tissue samples were respectively selected from the Genotype-Tissue Expression (GTEx) Project portal (dbGaP accession number phs000424.v8.p2), and from the PanCancer Genome Atlas (accession number EGAS00001001692), respectively. Data were log2 normalized, quantile normalized, and collapsed by using median values, using Phantasus **v1.11.0** software.

For scRNA-Seq analysis, multiple datasets of normal and tumor origin were analyzed (bone marrow from healthy volunteers and AML patients: GSE1166256-6; colorectal cancer patients: GSE144735; breast normal and tumor tissues: GSE164898; non–squamous cell lung carcinoma: E-MTAB-8107; hepatocellular carcinoma: GSE 140228; basocellular carcinoma: GSE11625; and renal cell carcinoma: phs002065.v1.p1). Data were log2, batch effect was corrected using mutual nearest neighbors (MNN) method, only transcripts found in more than 5 cells and expressed in more than 200 cells were analyzed. The fraction of transcripts from mitochondrial genes was set up to 5% for normal tissues study and 10% for the tumor tissue study. Identification of subpopulations was realized using UMAP algorithm and was analyzed using Bioturing software.

Flow cytometry

The relative surface expression of BTN2A (107G3B5 and 7.48 mAbs) and BTN3A (20.1 and 108.5 mAbs) was assessed by flow cytometry using calibrator beads allowing for the quantification of antigen density (Quantum™ Simply Cellular® [QSC kits], Bang Laboratories, Fishers, IN). To avoid bias related to modulation of BTN surface expression in correlation analysis, relative quantification of BTN was performed concurrently with functional assays. Gating strategy of ALL blasts was described in the Supplementary Fig S1.

To analyze CD107 expression, Vγ9Vδ2 T cells and target cells were cocultured in a E:T ratio of 1:1 with anti-CD107a (clone H4A3, BD Biosciences), anti-CD107b (clone H4B4, BD Biosciences) and Golgi stop (Cat#554724, BD Biosciences), with 107G3B5 or isotype control (1 µg/mL). After 4 hours, cells were collected and analyzed by flow cytometry. To study IFNγ and TNFα production, cells were

permeabilized with Permwash (BD Biosciences) to allow intracellular staining. Cells were acquired on a BD FACS CANTO II (BD Biosciences) and analyzed using Flowjo software V10.6.2 (BD Biosciences).

Tumor spheroid generation

HT-29, PC-3 and Ishikawa cell lines were cultured to form spheroids. Depending on the type of functional assay, $1x10^4$ to 2 $x10^5$ cells were plated in 96 well low-attachment U-bottom plates (Costar) in cell culture medium containing 10% FBS. Cells were incubated for 5 days at 37°C and 5% $C0_2$ before use in functional assays.

Fluorescence Resonance Energy Transfer (FRET) experiments

FRET experiments were performed as described in Cano et al. (9). Briefly, eCFP- or eYFP- BTN2A1 (NM_007049.5) or BTN3A1 (NM_007048) fusions were cloned into into pCDN3.1-Zeo+ backbone (InvitrogenTM). HEK-293T cells were transiently transfected with eCFP and eYFP fusion proteins using lipofectamine 2000 reagent (InvitrogenTM) according to manufacturer's instruction and analyzed by flow cytometry 20–24 h post-transfection using a CytoFLEX (Beckman Coulter). eYFP signal was recorded using the 488 nm laser with a 525/50 filter, eCFP signal was recorded using the 405 nm laser with a 450/50 filter and FRET signal was recorded using the 405 nm laser with a 525/50 filter. Co-transfection of equal amounts of eCFP and eYFP was used to establish the background FRET levels whereas transfection of an eCFP–eYFP fusion protein serves to define FRET-positive cells according to Banning et al (35). For assessment of the impact of anti-BTN2A1 on BTN2A1/BTN3A1 complex, cells were transfected concomitantly with BTN2A1-eCFP and BTN3A1-eYFP and treated with cycloheximide (10 µg/mL, Sigma) and bafilomycin A1 (0.1 µM, Invivogen) for 6 hrs, then incubated with the indicated concentrations of anti-BTN2A1 and anti-BTN3A.

Live-cell imaging of 3-dimensional (3D) tumor spheroids

After 5 days of spheroid generation, PC-3 were incubated for 4 hours in serum-free medium containing calcein (Sigma) at a final concentration of 2 µM. PC-3 spheroids were then washed extensively and cocultured with Vγ9Vδ2 T cells from 6 HV for 48 hours at an E:T ratio of 5:1, in presence of an isotype control or 107G3B5 (10µg/mL).

Spheroid disruption was monitored by imaging calcein fluorescence every hour using the IncuCyte Zoom™ system (Essen Biosciences, objective 4X). Images were processed and analysed using IncuCyte Control software (Essen Biosciences) creating mask to obtain fluorescence area per image and spheroids illustrations contrast were performed using ImageJ software.

Apoptosis assays

Cell lines and primary ALL blasts

Target cells were first labelled with the Cell Proliferation Dye eFluor™ 670 (Thermo Fisher Scientific) and then cocultured for 4, 6 or 10 hours with effector cells at an E:T ratio of 5:1 (cell lines), 10:1 or 15:1 (primary ALL blasts), in the presence of an isotype control, 107G3B5 or anti-BTN3A 20.1 agonist mAb (1 or 10 µg/mL). In caspase assays, cell lines preincubated overnight with ZOL (45 µM) were used as a positive control. At the end of coculture, target cells were labeled with CellEvent™ caspase-3/7 green detection reagent (Thermo Fisher Scientific) for 30 min and analyzed by flow cytometry (BD FACSCanto II). The percentage of specific apoptosis was calculated using the formula [(experimental – spontaneous caspase 3/7 activation)/ (100 – spontaneous caspase 3/7 activation) x 100]. Apoptosis was also assessed by labeling target cells with Annexin-V (Miltenyi) and 7-AAD (BD Biosciences) for 10 minutes.

Tumor spheroids

Ishikawa, HT-29, PC-3 and CaSki were cocultured with Vγ9Vδ2 T cells from 6 HV for 10 hours at an E:T ratio of 5:1, in the presence of an isotype control or 107G3B5 (10µg/mL). Caspase-Glo 3/7 reagent was added at the end of the coculture and was incubated for 1 hour. Luminescence was quantified within 30 minutes using a CLARIOstar microplate reader.

Transient Transfection

HEK293T CRISPR knockouts for BTN2A and BTN3A were transiently transfected with different combinations of the following plasmids described in De Gassart et al. (25); pcDNA3.1_BTN2A1_link_eCFP, pcDNA3.1_BTN2A1_deltaB30.2_eCFP, pcDNA3.1_BTN3A1-link_eYFP, pcDNA3.1_BTN3A1_deltaB30.2e_YFP. Transfection reagent PEI max reagent (Thermo Fisher Scientific) was used according to the manufacturer's instructions. After 48h of incubation cells were co-cultured with expanded Vγ9Vδ2 T cells (E:T ratio of 1:1) in the presence of IgG1 or 107G3B5 (10 µg/mL). In some assays HEK293T cells were pretreated with ZOL (45 µM).

ELISA

Vγ9Vδ2 T cells and target cells were cocultured at an E:T ratio of 10:1. Supernatants were collected and frozen at -80°C for subsequent cytokine measurement. Supernatants were analyzed for TNFα and/or IFNγ production using respectively BD OptEIA Human TNFα and IFNγ ELISA kits (BD Biosciences, San Jose, CA). Flat-bottom 96-well plates (COSTAR) were coated with capture Ab overnight and then blocked with PBS (phosphate-buffered saline) 10% FCS for 1h. After 2h of incubation with standards or supernatants, plates were incubated with detection Ab and streptavidin HRP and then developed using 3,3',5,5'-tetramethylbenzidine (TMB) Liquid Substrate System (BD biosciences). The reaction was stopped with HCL 2N, and the absorbance was quantified within 30 minutes using a CLARIOstar microplate reader (BMG LABTECH, Champigny-sur-Marne, France) at a wavelength of 450 nm.

Recombinant Vγ9Vδ2 TCR binding assays

A recombinant Vγ9Vδ2 TCR (clone G115) (36) with a C-terminal Fc-tag or His-tag on the Vγ9 chain was produced in CHO cells, then purified using protein A column chromatography followed by buffer-exchange into PBS (Custom made by MImAbs SAS). Vγ9Vδ2 TCR were biotinylated using protein

labeling kit according to the manufacturer's instructions (FluoReporter® Mini-biotin-XX Protein Labeling kit, Thermofisher). Biotinylated proteins were then tetramerized with streptavidin-APC (Biolegend, San Diego, CA) at 4:1 molar ratio by adding the streptavidin over 10 times intervals to maximize tetramer formation. HEK293T, SUP-T1 or Ishikawa cells were saturated with 107G3B5 or isotype control (10 µg/mL) for 4 hours at 37°C. The cells were then stained with recombinant tetrameric Vγ9Vδ2 TCR-Fc at 10 µg/ml for 30min at 37°C. After two washes, AF647 mean fluorescence intensity (MFI) was assessed by flow cytometry (BD LSRFortessa, BD Biosciences).

Confocal microscopy

To study the colocalization of BTN2A1 and BTN3A1, we used two plasmids described in Cano et al. (9); pcDNA3.1_BTN3A1_link_eGFP plasmid et al and pcDNA3.1_BTN2A1_link_eCFP, which we modified by replacing eCFP by mcherry using in-fusion cloning kit (Takara). HEK293T cells were transiently transfected with either with BTN3A1 GFP or BTN2A1 mcherry using PEI max reagent (Thermo Fisher Scientific), according to the manufacturer's instructions. For both constructs, a linker was inserted between the BTN2A1/BTN3A1 C-terminal end and the -eGFP or -mCherry molecules in order to provide flexibility and not interfere with molecular function. The next day, the cells were plated on precoated coverslips with poly-L-lysine. After overnight incubation, cells were preincubated with either an isotype control or anti-BTN2A 107G3B5/7.48 or anti-BTN3A 20.1 (10µg/mL) for 1 hour. After two washes, cells were fixed with 3% paraformaldehyde in PBS (pH 7.4), saturated with 2% BSA in PBS (pH 7.4) for 2 hours and labeled with DAPI (Cat#D1309, Invitrogen) for 2min. After 2 washes with PBS and 1 wash with deionized water, coverslips were mounted with prolong Gold (Invitrogen). Cells were imaged using an inverted ZEISS LSM 880-Spectral-Airyscan (Oberkochen, Germany) with the 63X objective. BTN2A1 and BTN3A1 distribution and colocalization were analyzed using ImageJ software and the JACoP plugin.

To visualize and quantify the colocalization of BTN2A and BTN3A and the binding of the Vγ9Vδ2 TCR on a more relevant model, SUP-T1 cells were preincubated with either an isotype control or 107G3B5

(10µg/mL) or HMBPP (E-4-Hydroxy-3-methyl-but-2-enyl diphosphate, 10µM) for 4 hours at 37 °C. After two washes, cells were incubated with either an anti BTN2A 7.48 AF647or anti-BTN3A 103.2 AF488 (10µg/mL) for 1 hour at 4°C or with Vγ9Vδ2 TCR- Fc at 10 µg/ml for 30min at 37°C. After two washes, cells were fixed, then mounted with prolong Gold and covered with a coverslip overnight. Cells were imaged using an inverted ZEISS LSM 880-Spectral-Airyscan with the 63X objective.

Western blotting

8 million target cells (T)—697 and Ishikawa—were cocultured with Vγ9Vδ2 T cells expanded from healthy volunteers cells (E:T ratio = 2:1 for 697, 3:1 for Ishikawa) for 4 hours in RMPI with 10% FBS. Isotype control antibody mouse IgG1 (Miltenyi) or BTN2A1-specific antibody 107G3B5 was added to the final concentration of 10 µg/mL. In some experiments target cells were pretreated during 1h30 with z-DEVD-FMK (Cat#550378, BD Pharmingen) before coculture. After incubation, cells were washed in PBS and lysed in RIPA lysis buffer (Thermo Scientific). The protein concentrations were determined using Bradford reagent. Then, the proteins were run on an SDS-PAGE gel and transferred to PVDF membrane which were blocked in 5% milk and probed overnight with antibodies: anti α-tubulin (Clone 11H10, cell signaling) and anti-GSDME (Clone E2X7E, cell signaling). Secondary antibody conjugated with biotin and third antibody conjugated with horseradish peroxidase were followed by enhanced chemiluminescence (Cytivia). Results were confirmed by at least three independent experiments and quantified using Fiji.

Statistics

All analyses were performed using the Graph Pad Prism 5.0 (Graph Pad Software, San Diego, CA). The normality distribution of the data was determined by using the D'Agostino test. Appropriate statistical tests were used as indicated in the figure legends. All replicates' data are biological except for ELISA experiments, where technical replicates are indicated.

Data Availability

The datasets used and/or analyzed during the current study are available in the manuscript and its supplementary files or from the corresponding author upon reasonable request. Raw data underlying main text and supplementary figures are provided in Supplementary Raw Data Excel File S1.

Results

Targeting BTN2A1 with the agonist Ab 107G3B5 strengthens Vγ9Vδ2 T-cell killing and cytokine production

Expression of BTN2A was investigated at the transcriptomic level in normal and tumor tissues (Supplementary Fig. S2a and b). BTN2A1 was widely expressed with a great heterogeneity across tissues and tumor subtypes (Supplementary Raw Data Excel File S1), with a distinct expression pattern compared to BTN2A2 and BTN3A1. Using publicly available scRNA-Seq datasets of tissues of normal and tumor origin, BTN2A1 was found ubiquitously expressed in immune and non-immune cells (Supplementary Fig. S2c). As previously described (9), the relative surface abundance of BTN2A1 on cell lines revealed a wide distribution in both hematological and solid cancer cell lines (Supplementary Fig. S3a,b). BTN2A1 was also found at the membrane of PB blasts from 28 ALL patients at diagnosis (Supplementary Fig. S3c). These data demonstrate that BTN2A1 is ubiquitously expressed at the transcript and protein level, and that it is found on the cell surface of tumors of different origins, including primary tumor cells.

Using HEK293T and KARPAS-299 cell lines, we observed that the BTN2A1-specific mAb 107G3B5 bound to control cells but not BTN2A KO cells, demonstrating the specificity of the antibody (Fig. 1a,b, Supplementary Fig. S4). We used two controls; an anti-BTN2A called 7.48, which has been well characterized and previously reported (9), and the anti-BTN3A 20.1.

Given the recently described key role of BTN2A1 in the activation of Vγ9Vδ2 T cells (9,12), we hypothesized that an agonistic anti-BTN2A1 may enhance the cytotoxic functions of Vγ9Vδ2 T cells. We first generated mAbs against the ectodomain of BTN2A1 by mouse immunization. Hybridoma

culture supernatants displaying the highest affinity for BTN2A1 underwent two rounds of selection for their ability to enhance Vγ9Vδ2 T-cell degranulation against Daudi cells (Fig. 1c). The anti-BTN2A1 encoded by this sequence was named 107G3B5. We then sought to further characterize the agonistic activity of 107G3B5 on Vγ9Vδ2 T-cell cytotoxicity.

Apoptosis assays of hematological cancer cell lines revealed that 107G3B5 and ZOL pretreatment significantly increased Vγ9Vδ2 T cell–mediated apoptosis to a similar extent (Fig. 1d), with different susceptibility profiles between cell lines (Fig. 1e). An increased activity of 107G3B5 was observed over time (Fig. 1f). To better characterized cell death, as caspase-3/7 activation could cause both non-proinflammatory and proinflammatory cell death, we performed 7-AAD/Annexin V staining. Using primary ALL blasts and 4 cancer cell lines co-cultured with Vγ9Vδ2 T cells, we observed that 107G3B5 treatment was associated with an increased proportion of Annexin V^+ target cells that were either negative or positive for 7AAD (Supplementary Fig. S5a and b). This result means that the 107G3B5 antibody induces not only apoptosis but also a lytic cell death. In addition, 107G3B5 improved both degranulation and production of TNFα and IFNγ by Vγ9Vδ2 T cells cocultured with hematological cell lines (Supplementary Fig. S6).

To determine if the activation mediated by 107G3B5 antibody was dependent on pAgs, HEK293T CRISPR knockouts for BTN2A and BTN3A were transiently transfected to express combinations of wild-type (WT) BTN3A1 and BTN2A1 or variants lacking their B30.2 domain (ΔB30.2). These cells were co-cultured with expanded Vγ9Vδ2 T cells in the presence of IgG1 or 107G3B5. In some assays HEK293T cells were pretreated with ZOL. Activation of Vγ9Vδ2 T cells was assessed by measuring human (Supplementary Fig. S7). As expected, pAg-mediated activation of Vγ9Vδ2 T cells was triggered only when BTN3A1 and BTN2A1 wild-type molecules were coexpressed. Like the anti-BTN3A 20.1 (37), the anti-BTN2A 107G3B5 induced the production of TNF-α and IFN-γ even if BTN2A1 or BTN3A1 lack their B30.2 domain, which demonstrates that the agonist anti-BTN2A1 functions independently of the involvement of pAgs.

To better describe the effects of 107G3B5 over time, holotomographic microscopy was used. This measures the spatial distribution of the RI of the observed biological object, here Vγ9Vδ2 T cells, which are small and dense in dry mass. As RI and dry mass content are linearly related, Vγ9Vδ2 T cells were the brightest on the RI image. Cancer cells were larger, had a lower dry mass density and therefore appeared darker on the RI image. Using AI, the RI signal alone was used for cell segmentation (Supplementary Fig. S8)(38). This label-free method (39) is a valid approach to further characterize apoptotic features (40). 107G3B5 treatment showed distinguishable Vγ9Vδ2 T-cell activation leading to SUP-T1 killing upon 107G3B5 treatment. In parallel, almost no apoptotic events were observed in the control condition (Fig. 1g, Supplementary Movies S1 and S2). We also confirmed our results by demonstrating an increase of the lethal fraction over time (Fig. 1h) and an increase in IFNγ production (Fig. 1i) after 107G3B5 treatment. Collectively, these findings suggest a broad effect of 1073B5 that may be related to the ubiquitous expression of BTN2A1 on various type of tumor cells(9).

107G3B5 improves allogeneic and autologous Vγ9Vδ2 T-cell function against primary ALL blasts

The antitumor functions of Vγ9Vδ2 T cells have been extensively studied in a variety of hematological malignancies (16,17,37,41,42) but have been less explored in ALL (14,43–45). Given the promising results obtained with 107G3B5 in ALL cell lines, we next sought to investigate whether 107G3B5 may enhance the functions of allogeneic Vγ9Vδ2 T cells against primary ALL blasts. Compared to the control condition, 107G3B5 increased Vγ9Vδ2 T cell–mediated apoptosis of 17 primary ALL blasts (Fig. 2a). As noted above, a lytic cell death was observed in coculture of Vγ9Vδ2 T cell with 4 primary ALL blasts (Supplementary Fig. S5c). As we found for hematological cell lines, 107G3B5 enhanced the degranulation and Th1 cytokine production capacity of Vγ9Vδ2 T cells cocultured with primary ALL blasts (Fig. 2b). This agonistic effect increased over time (Fig. 2c-e).

Using ZOL stimulation combined with IL-2 plus IL-15 for 14 days, we expanded Vγ9Vδ2 T cells from PBMCs of ALL patients. In one patient, Vγ9Vδ2 T-cell expansion allowed further testing of their

cytotoxic capacity, which was improved after treatment of the expanded cells with 107G3B5 (Fig. 2f). As in allogeneic assays, 107G3B5 increased degranulation and cytokine secretion of Vγ9Vδ2 T cells expanded from 4 ALL patients (Fig. 2g).

These findings consolidate the previous results obtained on cell lines, as we show that 107G3B5 treatment enhances both allogeneic and autologous Vγ9Vδ2 T-cell functions against primary ALL blasts.

107G3B5 sensitizes Vɣ9Vδ2 T-cell cytotoxicity in 3D tumor spheroid models

Next, we evaluated the activity of 107G3B5 in a solid tumor setting. Using cell lines of different tumor origins, we found that 107G3B5 significantly increased Vγ9Vδ2 T cell–mediated killing compared to the control condition (Fig. 3a; Supplementary Fig. S5d). To assess 107G3B5 activity in a relevant solid tumor model, we further investigated the effect of 107G3B5 on Vγ9Vδ2 T-cell effector functions using 3D spheroid assays and demonstrated that 107G3B5 increased significantly Vγ9Vδ2 T cell–mediated apoptosis of Ishikawa, HT-29 and PC-3 spheroids (Fig. 3b and c).

Live-cell fluorescence images of PC-3 spheroids co-cultured with Vγ9Vδ2 T cells from 6 HV showed a more pronounced decrease in calcein area over time after treatment with 107G3B5 compared to the control condition (Supplementary Fig. S9).

Analysis of the 24-hour coculture supernatant revealed a significant increase in IFNγ secretion after 107G3B5 treatment compared to the control condition (Fig. 3d). Consistent with the above findings, the PC-3 cell line appeared to be highly susceptible to Vγ9Vδ2 T cell–mediated killing after treatment with 107G3B5 (Fig. 3e).

We next used holotomographic microscopy to visualize the impact of 107G3B5 on the efficiency of Vγ9Vδ2 T cells to induce apoptosis in Ishikawa solid tumor cells. Consistent with previous results, we observed a rapid accumulation of apoptotic cells over time under 107G3B5 treatment, whereas no apoptotic features were distinguishable in the control condition (Fig. 3f, Supplementary Movies S3

and S4). The dead cells fraction was strongly increased upon 107G3B5 treatment (Fig. 3g) and was correlated with higher IFNγ production (Fig. 3h).

107G3B5 increases interactions between target cells and Vγ9Vδ2 T cells

To further characterize the mechanisms of action of 107G3B5, we assessed its impact on the interactions between Vγ9Vδ2 T cells and a hematological malignancy model, SUP-T1, and a solid cancer model, Ishikawa. Upon 107G3B5 treatment, we observed an increased proportion of Vγ9Vδ2 T cells in contact with a target cell in both cell lines (Fig. 4a). In addition, there was an increase in the target cell area covered by Vγ9Vδ2 T cells (Fig. 4b) and the average minimum distance between Vγ9Vδ2 and target cells (Fig. 4c). Conversely the movement of Vγ9Vδ2 cells was significantly decreased (Fig. 4d). These results suggest that 107G3B5 promotes contacts between Vγ9Vδ2 T cells and target cells and stabilizes their interactions. Different behaviors have been reported when T cells encounter antigen on the surface of antigen-presenting cells (APC), such as cessation of movement and the formation of a stable immunological synapse or continuous rapid movement from APC to APC (46). Accordingly, molecular interactions between Vγ9Vδ2 T cells and target cells are sufficient to induce the formation of an immunological synapse, but effector functions require the full engagement of the γδ TCR by a potent agonist (47). Altogether, our data indicate that 107G3B5 improved the quantity and the quality of interactions between target cells and Vγ9Vδ2 T cells over time, with subsequent increased cytotoxicity.

107G3B5 enhances binding of a recombinant Vγ9Vδ2 TCR on HEK293T, SUPT-T1 and Ishikawa cell lines

To gain insight into the underlying molecular mechanisms, we assessed whether 107G3B5 can directly affect the binding of a recombinant Vγ9Vδ2 TCR to target cells. First, using HEK293T, SUP-T1 and Ishikawa cell lines, we demonstrated by flow cytometry that 107G3B5 significantly increased Vγ9Vδ2 TCR binding to target cells (Fig. 5a and b). The binding of Vγ9Vδ2 TCR to SUP-T1 did not occur

diffusely but in specific areas of the target cells creating both mini and microclusters of fluorescence (Fig. 5c). 107G3B5 induced a significant increase in the number of Vγ9Vδ2 TCR miniclusters on the target cell surface (Fig. 5d). Consistent with our results, confocal microscopy experiments also showed that the 107G3B5 antibody induced BTN2A1 clustering using the SUP-T1 cell line (Supplementary Fig. S10). Treatment of target cells using the potent Vγ9Vδ2 activator HMBPP induced only microclusters of Vγ9Vδ2 TCR on the SUP-T1 surface. Taken together, our results show that 107G3B5 has its own unique mechanism of action by directly and strongly enhancing Vγ9Vδ2 TCR binding to various target cells in a BTN2A-clustering dependent manner.

To better understand the molecular mechanism, we investigated the effect of 107G3B5 on BTN3A1–BTN2A1 interactions. To this end, HEK293T cells were transfected with BTN3A1-GFP and BTN2A1-mCherry constructs and incubated with agonist anti-BTN2A1 107G3B5, antagonist anti-BTN2A1 7.48 or control isotype. 107G3B5 was able to significantly increase the colocalization of both molecules, (Supplementary Fig S11a). Indeed, the fraction of total BTN2A1 fluorescence that colocalized with BTN3A1 fluorescence was significantly increased on the HEK293T cell line after exposure to 107G3B5 (Supplementary Fig S11b). However, we observed no significant effect of the antagonist anti-BTN2A1 7.48 on BTN2A1–BTN3A1 clustering. Increased interactions between BTN2A1 and BTN3A1 were confirmed by an increasing FRET signal under increasing anti-BTN2A concentrations in BTN2A1KO/BTN3A1KO HEK293T cells transfected with CFP/YFP BTN2A1 and BTN3A1 fusion proteins, (Supplementary Fig S11c). The interaction of these two molecules is part of the mandatory first steps of Vγ9Vδ2 T-cell activation (10) and our results demonstrate that 107G3B5 promotes the colocalization of both molecules.

Vγ9Vδ2 T-cell activation by 107G3B5 triggers tumor cells pyroptosis

Because 107G3B5 increases interactions between target cells and Vγ9Vδ2 T cells we wanted to determine whether pyroptosis may contribute to 107G3B5 activity. Pyroptosis is orchestrated by the cleavage of Gasdermin (GSDM) family members such as GSDMD and GSDME. Indeed, GSDME, a

55kDa protein, can be cleaved by caspase-3/7 to produce a 35kDa active form that oligomerizes at the plasma membrane causing pore formation and subsequent cellular pyroptosis(28). When we co-incubated Vγ9Vδ2 T cells with SUPT-1, 697 or Ishikawa cell lines, we observed that 107G3B5 not only increased caspase 3/7 activation, but also increased tumor cell permeabilization via Live/Dead+ marker (Fig. 6a and b). To better understand whether pyroptosis might be involved in this permeabilization, we sought to visualize the GSDME forms by western blot. We observed that the full-length form of GSDME was expressed in the 697 and Ishikawa cell lines but was absent in Vγ9Vδ2 T cells (Fig. 6c). In target/effector co-cultures, we observed the full-length form of GSDME but also weakly the N-terminal active form, indicating that Vγ9Vδ2 T cells alone can induce GSDME cleavage. Moreover, the relative expression of the full-length form of GSDME was reduced with 107G3B5 treatment whereas the active form was significantly increased (Fig.6c and d). Taken together, these results suggest that 107G3B5 mediates the activation of Vγ9Vδ2 T cells, which can mobilize GSDME to induce pyroptosis within the target cell. We further demonstrated that z-DEVD, a well-known caspase 3-specific inhibitor, considerably decreased proteolytic cleavage of GSDME, showing that pyroptosis induced by 107G3B5 was caspase 3–dependent (Supplementary Fig S12).

Discussion

VγV9δ2 T cells provide a natural bridge between innate and adaptive immunity, responding rapidly and strongly to cancer cells or pathogenic infections. Expression of BTN2A1 is required to trigger activation of Vγ9Vδ2 T cells by pAgs. However, current data on BTN2A1 expression are very sparse. Indeed, BTN2A1 expression has been shown on circulating B cells, T cells, NK cells, monocytes and VγV9δ2 T cells from healthy volunteers(12). Expression on tumor was known for only a few cell lines (9). Here, we have demonstrated that BTN2A1 was ubiquitously expressed at the transcriptomic and protein level in normal and tumor tissues. Moreover, BTN2A1 was found on the cell surface of tumor from different origins including primary ALL tumor cells. Transcriptomic data highlight a distinct expression pattern of BTN2A1 compared to BTN3A1 in normal and tumor tissues, highlighting

the importance of having a non-BTN3A target such as BTN2A. We and our colleagues have also previously shown that an increased level of expression of BTN2A1 on primary AML blasts was associated with increased activity of the anti-BTN3A 20.1 (9).We therefore hypothesize that certain patients will respond better to one or the other of these antibodies, possibly due to the more or less strong expression of BTN3A or BTN2A and/or co-expression with molecules of activation or inhibition. The therapeutic armamentarium is expanding but there is a real need to identify biomarkers that will improve the selection of patients who will respond best to treatment, such as anti-BTN2A and anti-BTN3A.

Our results show that 107G3B5 improved the killing of cell lines from solid or hematologic origin and was also able to enhance both allogeneic and autologous Vγ9Vδ2 T-cell functions against primary cells. These findings suggest that BTN2A1 can be targeted in a wide range of tumors and should be considered as a novel immune checkpoint to target in cancer immunotherapy.

One limitation of our study could be to render all $BTN2A1^{+}$ and $BTN3A1^{+}$ cells sensitive to Vγ9Vδ2 T cells that could be responsible of off-target cytotoxicity and may limit the possibility of using the antibody as a therapeutic agent. However activated Vγ9Vδ2 T cells selectively kill tumor cells, which suggests that Vγ9Vδ2 T cells require a second signal for activation (48). It remains to be further elucidated if NKG2D or other coreceptors expressed on Vγ9Vδ2 T cells are involved in anti-BTN2A–induced selective cytotoxic activity toward cancer cells.

BTN2A1 is a surface protein that has been described as a key molecule that binds directly to the γ9 chain of the TCR. However, the molecular mechanisms involved in the regulation of Vγ9Vδ2 T-cell activation are still unclear. We have recently shown that BTN2A1 mAbs can inhibit the ability of Vγ9Vδ2 T cells to kill cancer cells(9). Indeed, BTN2A1 mAbs are able to completely prevent the binding of BTN2A1 to the Vγ9Vδ2 TCR. In contrast, we report here for that a unique anti-BTN2A, mAb 107G3B5, can induce Vγ9Vδ2 T-cell activation. Our work demonstrates that the binding of 107G3B5 to BTN2A1-expressing cells increases the interaction of recombinant Vγ9Vδ2 TCR. To better understand the underlying molecular mechanisms of action, we analyzed the impact of 107G3B5 on

BTN2A1 clustering and on its association with BTN3A1. We observed that upon 107G3B5 treatment, BTN2A1 appears to form clusters at the surface of cancer cells. Given that TCR avidity depends on both the affinity of a single TCR molecule for its ligand and the number of TCR–ligand engagements, we hypothesis that BTN2A1 clusters increase the avidity for Vγ9Vδ2 TCR. We do not exclude that other associated molecules may be directly required. Our findings support a model in which BTN2A1 is more than a passive interacting molecule, BTN2A1 appears to be an on/off switch molecule for Vγ9Vδ2 T cells. Therefore, BTN2A1 represents a fundamentally different class of immune recognition compared to the well-known antigen-presenting molecules such as MHC and MHC-like molecules.

The pAgs bind to the B30.2 intracellular domain of BTN3A1 and this has recently been defined as a key step in initiating an intracellular heterodimeric association between BTN3A1 and BTN2A1(10). Our results highlight that the anti-BTN2A1 agonist 107G3B5 functions completely independently of the involvement B30.2 and consequently of pAgs. However, we also demonstrate that 107G3B5 can enhance BTN2A1–BTN3A1 interactions. We did not rule out the possibility that their intracellular domains is involved in such phenomena. The involvement of intracellular or extracellular domains in the observed colocalization induced by the 107G3B5 should be further investigated.

Despite the growing importance of immunotherapy in cancer, its applications are severely limited by the fact that a high percentage of patients do not respond or respond only transiently. Many cancer tumors are not inflamed or "cold," meaning that the immune system does not recognize them. Induction of apoptosis has long been considered as one of the most important strategies for cancer treatment. Interestingly, the immunogenicity of tumor cells can be maximized by inducing non-apoptotic cell death. Indeed, recent studies have found that GSDME-mediated pyroptosis enhances the phagocytic function of tumor-associated macrophages on tumor cells and increases the number and function of tumor-infiltrating $CD8^+$ T cells and NK cells (27). In melanoma patients, a gene signature associated with increased pyroptosis was correlated with a better prognosis and was predictive of response to anti–PD-1 immunotherapy (49). Cytotoxic cells such as

NK cells, $CD8^+$ T cells and CAR T cells induce tumor cells death through pyroptosis (27,28). Here, we show that Vγ9Vδ2 T cells are able to convert non-inflammatory apoptosis into pyroptosis in GSDME-expressing cancer cell lines. Interestingly, pyroptosis induced by the GSDME cleavage is strongly enhanced by agonist anti-BTN2A1 treatment.

Tumor cell death by pyroptosis is often dampened by epigenetic silencing of GSDME due to hypermethylation of the GSDME promoter, which is found in approximately 52-65% of primary cancers (50). However, treatment with the demethylating agent 5-aza-2'-deoxycytidine or decitabine can induce the expression of GSDME (51,52). γδ T cells are attractive effector cells for cancer immunotherapy because they exert potent cytotoxicity against a wide range of cancer cells. Although these approaches have been well tolerated, the clinical responses have generally been infrequent and of short duration (53–56). In this context, enhancing immunogenic cell death such as pyroptosis appears to be a promising strategy to improve the efficacy of γδ T cell–based immunotherapy.

In conclusion, our results demonstrate that agonistic targeting of BTN2A is a promising option as it (i) allows the sensitization of ALL in both allogeneic and autologous settings as well as solid tumor models to Vγ9Vδ2 T cells, (ii) by quantitatively and qualitatively improving the interaction between target and effector cells, associated with (iii) BTN2A1 clustering and BTN3A1 colocalization, triggering (iv) the conversion of cancer cell apoptosis into inflammatory pyroptosis. Future work is needed to determine the potential role of other immune cytotoxic cell subsets. Finally, our findings demonstrate the great potential of targeting BTN2A for the treatment of cancer. Additional preclinical data will guide the future development of anti-BTN2A treatments. It is tempting to speculate that this discovery may help to improve clinical outcomes for patients with cancers, including non-inflammatory tumors.

Acknowledgments

We thank the IPC Immunomonitoring platform and the the IPC Tumor Bank (authorization number AC-2007-33, granted by the French Ministry of Research). We thank the Timone Microscopy platform

PIVMI from the Center for Cardiovascular and Nutrition Research. The team “Immunity and Cancer” was labeled “FRM DEQ20180339209” (for D.O.). A.C.L.F was funded by the Poste d’Accueil INSERM from November 2019 to October 2021. We would like to thank Mauro Modesti for advice.

Author contributions

A.C.L.F, C.I., C.E.C., M.F. and D.O. conceived and designed the study. A.C.L.F, C.I., N.B., L.G., S.F., F.O., A.L.R, L.C., L.D., C.D, A.A. and A.B. performed experiments. A.C.L.F, C.I., N.B., L.G., L.C., L.D., C.D., C.E.C., M.F. and D.O. interpreted the data. N.V. treated patients and coordinated the study. A.C.L.F, C.I., C.E.C, G.G, M.F. and D.O. coordinated the research and wrote the manuscript. All authors critically reviewed the manuscript.

References

1. Wilcox RA, Tamada K, Flies DB, Zhu G, Chapoval AI, Blazar BR, et al. Ligation of CD137 receptor prevents and reverses established anergy of CD8+cytolytic T lymphocytes in vivo. Blood. 2004;103:177–84.

2. Gao Y, Yang W, Pan M, Scully E, Girardi M, Augenlicht LH, et al. γδ T Cells Provide an Early Source of Interferon γ in Tumor Immunity. J Exp Med. 2003;198:433–42.

3. Tosolini M, Pont F, Poupot M, Vergez F, Nicolau-Travers M-L, Vermijlen D, et al. Assessment of tumor-infiltrating TCRVγ9Vδ2 γδ lymphocyte abundance by deconvolution of human cancers microarrays. Oncoimmunology. 2017;6:e1284723.

4. Gentles AJ, Newman AM, Liu CL, Bratman SV, Feng W, Kim D, et al. The prognostic landscape of genes and infiltrating immune cells across human cancers. Nat Med. 2015;21:938–45.

5. Gober H-J, Kistowska M, Angman L, Jenö P, Mori L, De Libero G. Human T cell receptor gammadelta cells recognize endogenous mevalonate metabolites in tumor cells. J Exp Med. 2003;197:163–8.

6. Tanaka Y, Morita CT, Tanaka Y, Nieves E, Brenner MB, Bloom BR. Natural and synthetic non-peptide antigens recognized by human γδ T cells. Nature. Nature Publishing Group; 1995;375:155–8.

7. Sandstrom A, Peigné C-M, Léger A, Crooks JE, Konczak F, Gesnel M-C, et al. The intracellular B30.2 domain of Butyrophilin 3A1 binds phosphoantigens to mediate activation of human Vγ9Vδ2 T cells. Immunity. 2014;40:490–500.

8. Yang Y, Li L, Yuan L, Zhou X, Duan J, Xiao H, et al. A Structural Change in Butyrophilin upon Phosphoantigen Binding Underlies Phosphoantigen-Mediated Vγ9Vδ2 T Cell Activation. Immunity. 2019;50:1043-1053.e5.

9. Cano CE, Pasero C, De Gassart A, Kerneur C, Gabriac M, Fullana M, et al. BTN2A1, an immune checkpoint targeting Vγ9Vδ2 T cell cytotoxicity against malignant cells. Cell Rep. 2021;36:109359.

10. Hsiao C-HC, Nguyen K, Jin Y, Vinogradova O, Wiemer AJ. Ligand-induced interactions between butyrophilin 2A1 and 3A1 internal domains in the HMBPP receptor complex. Cell Chem Biol [Internet]. 2022 [cited 2022 Jan 29]; Available from: https://www.sciencedirect.com/science/article/pii/S2451945622000046

11. Yuan L, Ma X, Yang Y, Li X, Ma W, Yang H, et al. Phosphoantigens are Molecular Glues that Promote Butyrophilin 3A1/2A1 Association Leading to Vγ9Vδ2 T Cell Activation [Internet]. bioRxiv; 2022 [cited 2022 Jun 1]. page 2022.01.02.474068. Available from: https://www.biorxiv.org/content/10.1101/2022.01.02.474068v1

12. Rigau M, Ostrouska S, Fulford TS, Johnson DN, Woods K, Ruan Z, et al. Butyrophilin 2A1 is essential for phosphoantigen reactivity by γδ T cells. Science [Internet]. 2020 [cited 2020 Feb 1]; Available from: https://science-sciencemag-org.proxy.insermbiblio.inist.fr/content/early/2020/01/08/science.aay5516

13. Karunakaran MM, Willcox CR, Salim M, Paletta D, Fichtner AS, Noll A, et al. Butyrophilin-2A1 Directly Binds Germline-Encoded Regions of the Vγ9Vδ2 TCR and Is Essential for Phosphoantigen Sensing. Immunity. 2020;52:487-498.e6.

14. Lança T, Correia DV, Moita CF, Raquel H, Neves-Costa A, Ferreira C, et al. The MHC class Ib protein ULBP1 is a nonredundant determinant of leukemia/lymphoma susceptibility to γδ T-cell cytotoxicity. Blood. 2010;115:2407–11.

15. Gomes AQ, Correia DV, Grosso AR, Lança T, Ferreira C, Lacerda JF, et al. Identification of a panel of ten cell surface protein antigens associated with immunotargeting of leukemias and lymphomas by peripheral blood gammadelta T cells. Haematologica. 2010;95:1397–404.

16. Gertner J, Wiedemann A, Poupot M, Fournié J-J. Human gammadelta T lymphocytes strip and kill tumor cells simultaneously. Immunol Lett. 2007;110:42–53.

17. Gertner-Dardenne J, Castellano R, Mamessier E, Garbit S, Kochbati E, Etienne A, et al. Human Vγ9Vδ2 T Cells Specifically Recognize and Kill Acute Myeloid Leukemic Blasts. J Immunol. American Association of Immunologists; 2012;188:4701–8.

18. Corvaisier M, Moreau-Aubry A, Diez E, Bennouna J, Mosnier J-F, Scotet E, et al. V gamma 9V delta 2 T cell response to colon carcinoma cells. J Immunol Baltim Md 1950. 2005;175:5481–8.

19. Cordova A, Toia F, La Mendola C, Orlando V, Meraviglia S, Rinaldi G, et al. Characterization of human γδ T lymphocytes infiltrating primary malignant melanomas. PloS One. 2012;7:e49878.

20. Viey E, Fromont G, Escudier B, Morel Y, Da Rocha S, Chouaib S, et al. Phosphostim-activated gamma delta T cells kill autologous metastatic renal cell carcinoma. J Immunol Baltim Md 1950. 2005;174:1338–47.

21. Kabelitz D, Wesch D, Pitters E, Zöller M. Characterization of tumor reactivity of human V gamma 9V delta 2 gamma delta T cells in vitro and in SCID mice in vivo. J Immunol Baltim Md 1950. 2004;173:6767–76.

22. Santolaria T, Robard M, Léger A, Catros V, Bonneville M, Scotet E. Repeated systemic administrations of both aminobisphosphonates and human Vγ9Vδ2 T cells efficiently control tumor development in vivo. J Immunol Baltim Md 1950. 2013;191:1993–2000.

23. Yazdanifar M, Barbarito G, Bertaina A, Airoldi I. γδ T Cells: The Ideal Tool for Cancer Immunotherapy. Cells [Internet]. 2020 [cited 2020 Oct 22];9. Available from: https://www.ncbi.nlm.nih.gov/pmc/articles/PMC7290982/

24. Sebestyen Z, Prinz I, Déchanet-Merville J, Silva-Santos B, Kuball J. Translating gammadelta (γδ) T cells and their receptors into cancer cell therapies. Nat Rev Drug Discov. 2020;19:169–84.

25. De Gassart A, Le K-S, Brune P, Agaugué S, Sims J, Goubard A, et al. Development of ICT01, a first-in-class, anti-BTN3A antibody for activating Vγ9Vδ2 T cell-mediated antitumor immune response. Sci Transl Med. 2021;13:eabj0835.

26. Du T, Gao J, Li P, Wang Y, Qi Q, Liu X, et al. Pyroptosis, metabolism, and tumor immune microenvironment. Clin Transl Med. 2021;11:e492.

27. Zhang Z, Zhang Y, Xia S, Kong Q, Li S, Liu X, et al. Gasdermin E suppresses tumour growth by activating anti-tumour immunity. Nature. Nature Publishing Group; 2020;579:415–20.

28. Liu Y, Fang Y, Chen X, Wang Z, Liang X, Zhang T, et al. Gasdermin E-mediated target cell pyroptosis by CAR T cells triggers cytokine release syndrome. Sci Immunol. 2020;5:eaax7969.

29. Tan Y, Chen Q, Li X, Zeng Z, Xiong W, Li G, et al. Pyroptosis: a new paradigm of cell death for fighting against cancer. J Exp Clin Cancer Res CR. 2021;40:153.

30. García VE, Jullien D, Song M, Uyemura K, Shuai K, Morita CT, et al. IL-15 enhances the response of human gamma delta T cells to nonpeptide [correction of nonpetide] microbial antigens. J Immunol Baltim Md 1950. 1998;160:4322–9.

31. Aehnlich P, Carnaz Simões AM, Skadborg SK, Holmen Olofsson G, thor Straten P. Expansion With IL-15 Increases Cytotoxicity of Vγ9Vδ2 T Cells and Is Associated With Higher Levels of Cytotoxic Molecules and T-bet. Front Immunol. 2020;11:1868.

32. Van Acker HH, Anguille S, Willemen Y, Van den Bergh JM, Berneman ZN, Lion E, et al. Interleukin-15 enhances the proliferation, stimulatory phenotype, and antitumor effector functions of human gamma delta T cells. J Hematol OncolJ Hematol Oncol [Internet]. 2016;9. Available from: http://www.ncbi.nlm.nih.gov/pmc/articles/PMC5041439/

33. Compte E, Pontarotti P, Collette Y, Lopez M, Olive D. Frontline: Characterization of BT3 molecules belonging to the B7 family expressed on immune cells. Eur J Immunol. 2004;34:2089–99.

34. Forcina GC, Conlon M, Wells A, Cao JY, Dixon SJ. Systematic Quantification of Population Cell Death Kinetics in Mammalian Cells. Cell Syst. 2017;4:600-610.e6.

35. Banning C, Votteler J, Hoffmann D, Koppensteiner H, Warmer M, Reimer R, et al. A Flow Cytometry-Based FRET Assay to Identify and Analyse Protein-Protein Interactions in Living Cells. PLoS ONE. 2010;5:e9344.

36. Allison TJ, Winter CC, Fournié JJ, Bonneville M, Garboczi DN. Structure of a human gammadelta T-cell antigen receptor. Nature. 2001;411:820–4.

37. Benyamine A, Le Roy A, Mamessier E, Gertner-Dardenne J, Castanier C, Orlanducci F, et al. BTN3A molecules considerably improve Vγ9Vδ2T cells-based immunotherapy in acute myeloid leukemia. Oncoimmunology [Internet]. 2016 [cited 2018 Feb 11];5. Available from: https://www.ncbi.nlm.nih.gov/pmc/articles/PMC5087298/

38. Moreno H, Archetti L, Gibbin E, Grandchamp AE, Fréchin M. Artificial Intelligence-Powered Automated Holotomographic Microscopy Enables Label-Free Quantitative Biology. Microsc Today. Cambridge University Press; 2021;29:24–32.

39. Sandoz PA, Tremblay C, van der Goot FG, Frechin M. Image-based analysis of living mammalian cells using label-free 3D refractive index maps reveals new organelle dynamics and dry mass flux. PLoS Biol. 2019;17:e3000553.

40. Salucci S, Battistelli M, Burattini S, Sbrana F, Falcieri E. Holotomographic microscopy: A new approach to detect apoptotic cell features. Microsc Res Tech. 2020;83:1464–70.

41. Gundermann S, Klinker E, Kimmel B, Flierl U, Wilhelm M, Einsele H, et al. A comprehensive analysis of primary acute myeloid leukemia identifies biomarkers predicting susceptibility to human allogeneic Vγ9Vδ2 T cells. J Immunother Hagerstown Md 1997. 2014;37:321–30.

42. Aswald JM, Wang X-H, Aswald S, Lutynski A, Minden MD, Messner HA, et al. Flow cytometric assessment of autologous γδ T cells in patients with acute myeloid leukemia: Potential effector cells for immunotherapy? Cytometry B Clin Cytom. 2006;70B:379–90.

43. Siegers GM, Felizardo TC, Mathieson AM, Kosaka Y, Wang X-H, Medin JA, et al. Anti-leukemia activity of in vitro-expanded human gamma delta T cells in a xenogeneic Ph+ leukemia model. PloS One. 2011;6:e16700.

44. Duval M, Yotnda P, Bensussan A, Oudhiri N, Guidal C, Rohrlich P, et al. Potential antileukemic effect of gamma delta T cells in acute lymphoblastic leukemia. Leukemia. 1995;9:863–8.

45. Lamb Jr L, Musk P, Ye Z, van Rhee F, Geier SS, Tong J-J, et al. Human $\gamma\delta^+$ T lymphocytes have *in vitro* graft *vs* leukemia activity in the absence of an allogeneic response. Bone Marrow Transplant. 2001;27:601–6.

46. Dustin ML. Stop and go traffic to tune T cell responses. Immunity. 2004;21:305–14.

47. Favier B, Espinosa E, Tabiasco J, Dos Santos C, Bonneville M, Valitutti S, et al. Uncoupling between immunological synapse formation and functional outcome in human gamma delta T lymphocytes. J Immunol Baltim Md 1950. 2003;171:5027–33.

48. Harly C, Guillaume Y, Nedellec S, Peigné C-M, Mönkkönen H, Mönkkönen J, et al. Key implication of CD277/butyrophilin-3 (BTN3A) in cellular stress sensing by a major human γδ T-cell subset. Blood. 2012;120:2269–79.

49. Zhou B, Sha S, Tao J, Li J, Shen C, Zhu J, et al. The expression pattern of pyroptosis-related genes predicts the prognosis and drug response of melanoma. Sci Rep. 2022;12:21566.

50. de Beeck KO, Schacht J, Van Camp G. Apoptosis in acquired and genetic hearing impairment. Hear Res. 2011;281:18–27.

51. Akino K, Toyota M, Suzuki H, Imai T, Maruyama R, Kusano M, et al. Identification of DFNA5 as a target of epigenetic inactivation in gastric cancer. Cancer Sci. 2007;98:88–95.

52. Wang Y, Gao W, Shi X, Ding J, Liu W, He H, et al. Chemotherapy drugs induce pyroptosis through caspase-3 cleavage of a gasdermin. Nature. 2017;547:99–103.

53. Kunzmann V, Smetak M, Kimmel B, Weigang-Koehler K, Goebeler M, Birkmann J, et al. Tumor-promoting Versus Tumor-antagonizing Roles of γδ T Cells in Cancer Immunotherapy: Results From a Prospective Phase I/II Trial. J Immunother. 2012;35:205.

54. Kunzmann V, Bauer E, Feurle J, Florian Weißinger H-PT, Wilhelm M. Stimulation of γδ T cells by aminobisphosphonates and induction of antiplasma cell activity in multiple myeloma. Blood. 2000;96:384–92.

55. Wilhelm M, Smetak M, Schaefer-Eckart K, Kimmel B, Birkmann J, Einsele H, et al. Successful adoptive transfer and in vivo expansion of haploidentical γδ T cells. J Transl Med. 2014;12:45.

56. Bertaina A, Zorzoli A, Petretto A, Barbarito G, Inglese E, Merli P, et al. Zoledronic acid boosts γδ T-cell activity in children receiving αβ+ T and CD19+ cell-depleted grafts from an HLA-haplo-identical donor. Oncoimmunology. 2016;6:e1216291.

Table 1. Baseline patient and disease characteristics.

	All patients N = 28
Age, years	
Median [range]	48 [23-80]
>60 (%)	8 (28.6)
Gender	
Male (%)	14 (50)
Female (%)	14 (50)
WBC, $x10^9$/L	
Median [range]	76.1 [0.1-347]
High WBC count (%)	19 (67.8)
FAB subtype	
B (%)	19 (67.9)
B Ph- (%)	10 (52.6)
B Ph+ (%)	9 (47.4)
T (%)	9 (32.1)
PB blasts, %	
Mean (SD)	84.3 (9.6)
Induction (%)	28 (100)
CR after induction (%)	100 (100)
Allo-SCT (%)	14 (50)

Allo-SCT: allogenic hematopoietic stem cell transplantation in 1st complete remission; CR : complete remission; FAB : French-American-British classification; High WBC count : ≥ 30 $*10^9$/L for B lineage and ≥ $100*10^9$ for T lineage; Ph-: Philadelphia chromosome-negative ALL; Ph+: Philadelphia chromosome-positive ALL; PB : peripheral blood; WBC: white blood cells.

Figure Legends

Fig. 1. Anti-BTN2A1 107G3B5 enhances Vγ9Vδ2 T cell-mediated killing of a broad range of hematological cancer cell lines.

CRISPR-Cas9-mediated inactivation of BTN2A was performed in HEK293T (a) and KARPAS-299 (b) cell lines. BTN2A and BTN3A expression levels were assessed by flow cytometry. (c) Vγ9Vδ2 T cells expanded from healthy donor PBMCs (n=3) were co-cultured with Daudi cells (E: T ratio 1:1) in the presence of 50 µL of the indicated anti-BTN2A hybridoma supernatants and %CD107ab^{+} cells were assessed after 4h by flow cytometry. (d,e) Apoptosis of KARPAS, DAUDI, SUP-T1 and 697 cell lines, was evaluated by flow cytometry analysis of caspase 3/7 cleavage after 4-hour coculture with Vγ9Vδ2 T cells from 3 HV (E:T ratio 5:1) in the presence of an isotype control or the anti-BTN2A 107G3B5 (10µg/mL). Target cells preincubated over-night (O/N) with zoledronate (ZOL) (45 µM) were used as positive control. (f) Apoptosis of SUP-T1 and DAUDI was monitored by flow cytometry analysis of caspase 3/7 cleavage after 4, 6 and 10-hours of coculture with Vγ9Vδ2 T cells from 3 HV (E:T ratio 2:1) in the presence of an isotype control or the anti-BTN2A 107G3B5 (10µg/mL). (g) Sequence of snapshots depicting γδ T cells (E) coculture with SUPT1 (T; ratio T/E = 1/2) treated with 10ug/ml of mIgG1 control isotype (upper panel) or anti-BTN2A1 107G3B5 (down panel) within 20hours. The red arrows indicate apoptotic cells. (h) Quantification of lethal fraction. (i) IFNγ concentration in the culture supernatants at the end of the acquisition. Means ± s.e.m. pooled from one experiment (d,e) or two experiments (f) are depicted. Statistical significance was established using one-way Anova with Tukey's post-test (d), Friedman test with Dunn's post-test (e) or two-way Anova with Tukey's post-test (f). *p< 0.05; ***p < 0.001; ****p < 0.0001

Fig. 2 107G3B5 improves allogeneic and autologous effector response of Vγ9Vδ2 T cells against primary lymphoblastic blasts. (a) Apoptosis of 17 primary ALL blasts was assessed by analysis of caspase 3/7 cleavage after 4-hour coculture with Vγ9Vδ2 T cells from 3 HV (E:T ratio 15:1) with either isotype control or 107G3B5 (10µg/mL). (b) Effector functions of Vγ9Vδ2 T cells (HV, n=2 or 3) were

assessed after a 4 hour co-culture with 17 primary ALL blasts (E:T ratio 1:1) in the presence of 107G3B5 or its isotype control (1µg/mL). Pooled from 6 independent experiments (a,b). (c,d) Apoptosis of 4 primary ALL blasts was monitored by analysis of caspase 3/7 cleavage after 4 and 10-hours coculture with Vγ9Vδ2 T cells from 3 HV (E:T ratio 10:1) in the presence of an isotype control, 107G3B5 or the anti-BTN3A agonist 20.1 (10µg/mL). Pooled from one experiment. (e) IFNγ concentration in supernatants of 24 and 48-hour coculture of Vɣ9Vδ2 T cells from 6 HV with 3 primary ALL blasts either with isotype control or 107G3B5 (10µg/mL). (f) Apoptosis of primary ALL blasts (n=1) was evaluated by analysis of caspase 3/7 cleavage after a 4-hour coculture with autologous Vγ9Vδ2 T cells (E:T ratio 10:1), in the presence of isotype control, 107G3B5 or the anti-BTN3A agonist 20.1 (10µg/mL). The experiment was performed in triplicate. (g) Effector functions of Vγ9Vδ2 T cells (n=4) were assessed by flow cytometry after a 4 hours co-culture with autologous primary ALL blasts (E:T ratio 1:1) in the presence of 107G3B5 (10µg/mL) or its isotype control. Pooled from 4 independent experiments. Means ± s.e.m. are depicted (a,b,c,d,e,f,g). The statistical significance was established using a paired T-test (a), Wilcoxon test (b,g), two-way anova test (c,d,e) *p< 0.05; **p < 0.01; ****p < 0.0001

Fig. 3. Anti BTN2A1 107G3B5 increases interactions between target cells and Vγ9Vδ2 T cells. (a) Apoptosis of 2D solid cancer cell lines (HT-29, PC-3) was assessed by flow cytometry analysis of caspase 3/7 cleavage after 10-hour coculture with Vγ9Vδ2 T cells from 5 HV (E:T ratio 5:1) in presence of an isotype control, 107G3B5 mAb (10µg/mL). Histograms represent the means ± s.e.m. pooled for two cell lines from two experiment. (b,c) Caspase 3 and 7 activity of tumor spheroids (Ishikawa, HT-29, PC-3) after 24-hrs coculture with Vγ9Vδ2 T cells from 6 HV (E:T ratio 5:1) in the presence of an isotype control, 107G3B5 mAb (10µg/mL). Luminescence is normalized by subtracting spontaneous caspase 3/7 activity for each spheroid. Box-plots of pooled luminescence for the three tumor spheroids (b) or histograms representing mean luminescence ± s.e.m. of each tumor spheroid

(c) are depicted. (d,e) IFNγ concentration in supernatants of 24-hour coculture of Vγ9Vδ2 T cells (HV, n=5 or 6) with 3D spheroids from Ishikawa, HT-29, and PC-3 cell lines (E:T ratio 15:1) with either isotype control or 107G3B5 mAb (10µg/mL). Box-plots of pooled IFNγ concentration for the three tumor spheroids (d) or histograms representing mean IFNγ concentration relative to control condition ± s.e.m. of each tumor spheroid (e). (f) Sequence of snapshots depicting γδ T cells cocultured with Ishikawa (E:T ratio 1:3) treated with 10µg/mL of mIgG1 control isotype (top panel) or anti-BTN2A1 107G3B5 (bottom panel) during 20hours. The red arrows indicate apoptotic cells. (g) Quantification of the lethal fraction in HTM videos (h) IFNγ concentration in the culture supernatants at the end of the acquisition. Experiments were performed in biological (b,c) or technical duplicate (d,e). The statistical significance was established using Kruskal-Wallis test with Dunn's post-test (a,e) or Wilcoxon test (b,c,d) . *p< 0.05; **p < 0.01.

Fig. 4 107G3B5 induces a strong increase in Vγ9Vδ2 TCR binding which is associated with BTN2A1 clustering (**a**) The ratio of γδ T cells in contact with target cells, (**b**) target cell area covered by γδ T cells in percentage, (**c**) the average minimal distance between γδ T cells centroid and target cells centroid and (**d**) the movement of γδ T cells in um/s were analyzed using a holotomography microscope. These four parameters were analyzed in γδ T cells (Effector: E) coculture with SUPT-1 (Target : T ; ratio T/E = 1/2) or Ishikawa (ratio 1/3) treated with 10ug/ml of mIgG1 control isotype (in black) or anti-BTN2A1 107G3B5 (in red). Acquisitions were performed each 9min for 20 hours. The boxplots represent for each condition the cumulative results of the acquisition between 4 and 20hours. The statistical significance was established using paired T test. ****p < 0.0001

Fig. 5 107G3B5 induces a strong increase in Vγ9Vδ2 TCR binding which is associated with BTN2A1 clustering. (**a,b**) Binding of a recombinant, tetramerized Vγ9Vδ2 TCR to HEK293T, SUP-T1 or Ishikawa, following saturation with 107G3B5 or an isotype control. Binding of Vγ9Vδ2 TCR (5µg/mL)

(**a**) or dose dependent binding was monitored by flow cytometry (**b**). (**c**) Confocal microscopy of tetramerized Vγ9Vδ2 TCR binding to SUP-T1, with or without previous saturation with an isotype control, 107G3B5 or HMBPP (**d**). Evaluation of Vγ9Vδ2TCR binding by quantification of dots observed after treatment with IgG1 control isotype or 107G3B5. Statistical significance was established using Wilcoxon test (**a**) or Mann Whitney test (**d**). **p < 0.01; ***p < 0.001.

Figure 6. Activation of Vγ9Vδ2 T cells by 107G3B5 induces cancer cell pyroptosis. Vγ9Vδ2 T cells were cocultured with SUPT-1, 697 or Ishikawa cells at an effector/target ratio (E/T), 2/1, 2/1 and 3/1, respectively. A control condition without Vγ9Vδ2 T cells was added called WO GD. Cells were treated with 10ug/ml of mIgG1 control isotype or anti-BTN2A1 107G3B5 for 5 hours. The percentage of activated caspase 3/7+ and or permeabilized Live/Dead + tumor cells was determined by flow cytometry. (**a**) Representative staining. (**b**) Data are means ±SD of 3 independent experiments (n>5). The statistical significance was established using a paired T-test. (**c,d**) GSDME and α-tubulin were analyzed by Western blot. (**c**) Visualization of representative Western blot. (**d**) Data are means of relative quantification ±SD of 4 independent experiments. Statistical significance was established using a paired T-test. *p< 0.05; **p < 0.01; ***p < 0.001; ****p < 0.0001.

Figure 1

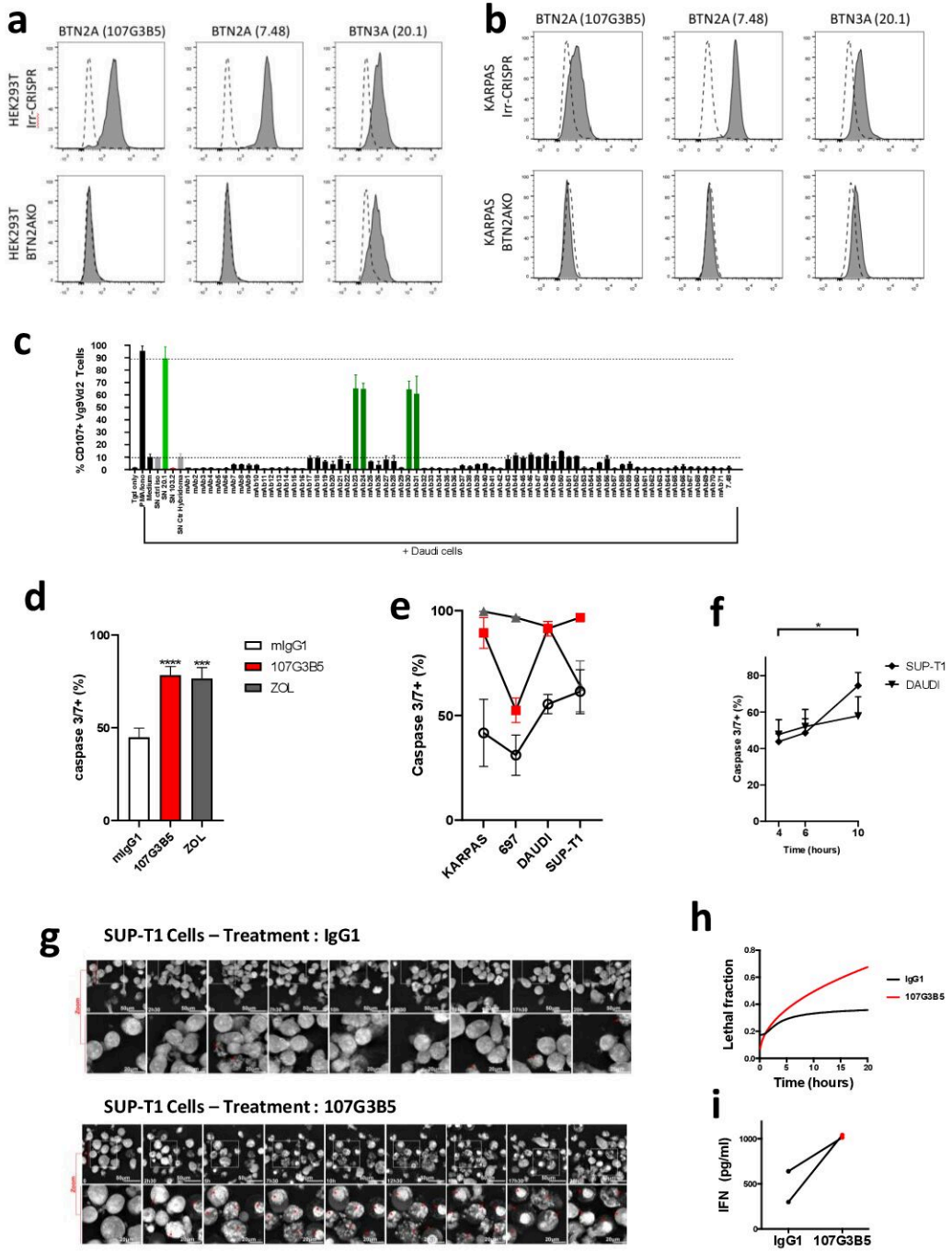
a
BTN2A (107G3B5)
BTN2A (7.48)
BTN3A (20.1)
HEK293T Irr-CRISPR
HEK293T BTN2AKO
b
BTN2A (107G3B5)
BTN2A (7.48)
BTN3A (20.1)
KARPAS Irr-CRISPR
KARPAS BTN2AKO
c
% CD107+ Vg9Vd2 Tcells
+ Daudi cells
d
caspase 3/7+ (%)
mIgG1
107G3B5
ZOL
e
Caspase 3/7+ (%)
KARPAS
697
DAUDI
SUP-T1
f
Caspase 3/7+ (%)
Time (hours)
SUP-T1
DAUDI
g
SUP-T1 Cells – Treatment : IgG1
SUP-T1 Cells – Treatment : 107G3B5
h
Lethal fraction
Time (hours)
IgG1
107G3B5
i
IFN (pg/ml)
IgG1
107G3B5

Figure 2

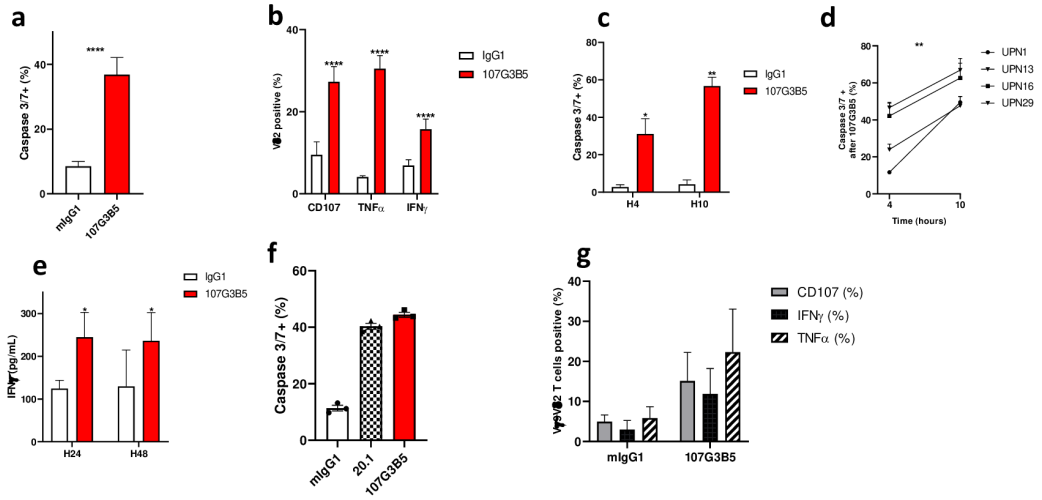
a
Caspase 3/7+ (%)
mIgG1
107G3B5
b
Vδ2 positive (%)
CD107
TNFα
IFNγ
IgG1
107G3B5
c
Caspase 3/7+ (%)
H4
H10
IgG1
107G3B5
d
Caspase 3/7 + after 107G3B5 (%)
Time (hours)
UPN1
UPN13
UPN16
UPN29
e
IFNγ (pg/mL)
H24
H48
IgG1
107G3B5
f
Caspase 3/7+ (%)
mIgG1
20.1
107G3B5
g
Vγ9Vδ2 T cells positive (%)
mIgG1
107G3B5
CD107 (%)
IFNγ (%)
TNFα (%)

Figure 3

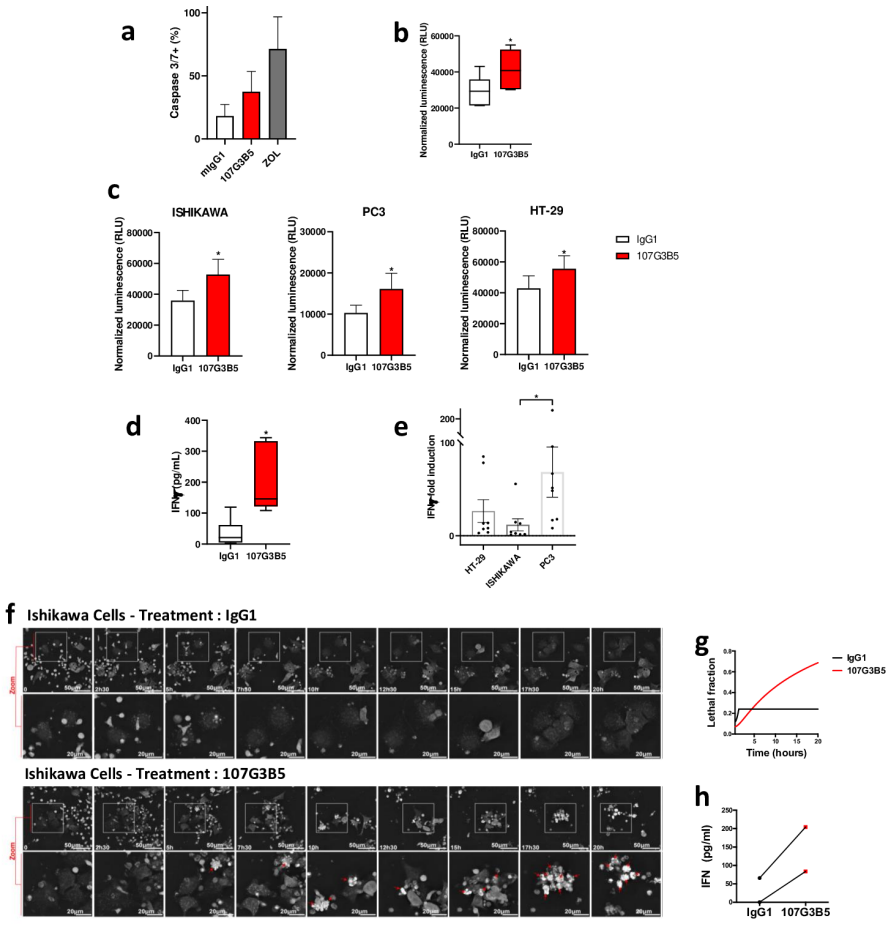
a
Caspase 3/7+ (%)
mIgG1
107G3B5
ZOL
b
Normalized luminescence (RLU)
IgG1
107G3B5
c
ISHIKAWA
PC3
HT-29
Normalized luminescence (RLU)
IgG1
107G3B5
d
IFNγ (pg/mL)
e
IFNγ fold induction
HT-29
ISHIKAWA
PC3
f
Ishikawa Cells - Treatment : IgG1
Ishikawa Cells - Treatment : 107G3B5
g
Lethal fraction
Time (hours)
IgG1
107G3B5
h
IFN (pg/ml)
IgG1
107G3B5

Figure 4

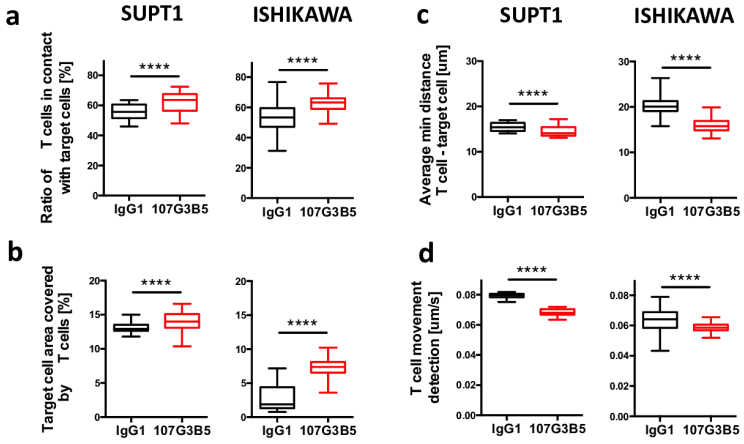
a
SUPT1
ISHIKAWA
Ratio of T cells in contact with target cells [%]
****
IgG1 107G3B5
b
Target cell area covered by T cells [%]
c
Average min distance T cell - target cell [um]
d
T cell movement detection [um/s]

Figure 5

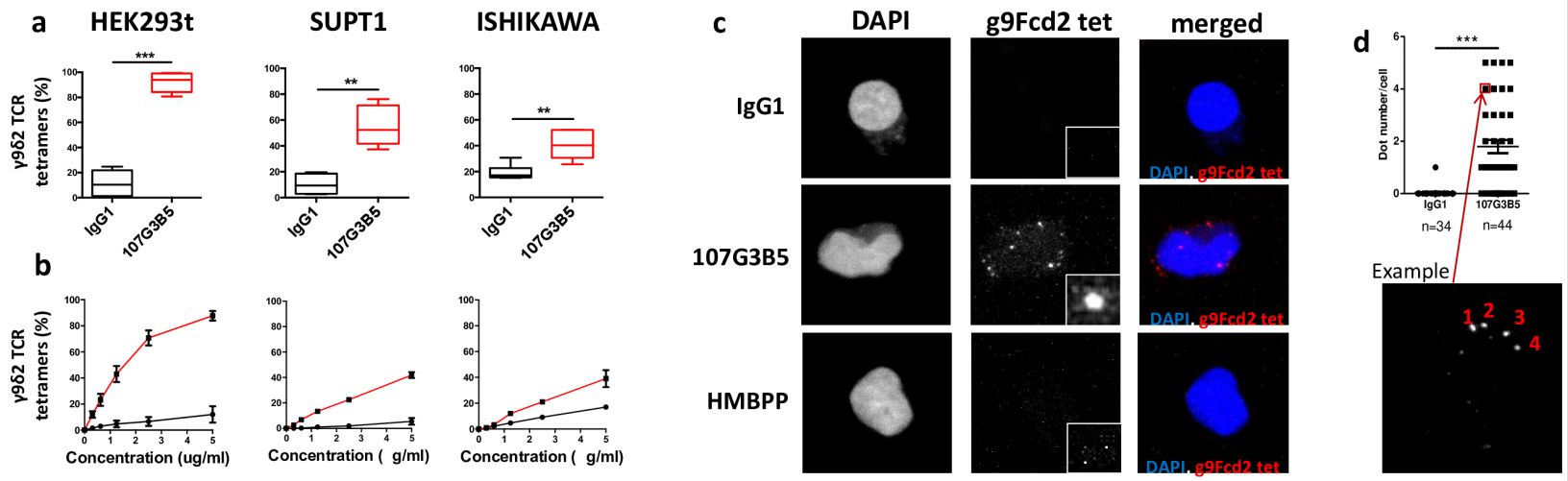
a
HEK293t
SUPT1
ISHIKAWA
γ9δ2 TCR tetramers (%)
IgG1
107G3B5
***
**
**
b
γ9δ2 TCR tetramers (%)
Concentration (ug/ml)
Concentration (g/ml)
Concentration (g/ml)
c
DAPI
g9Fcd2 tet
merged
IgG1
107G3B5
HMBPP
DAPI, g9Fcd2 tet
d
***
Dot number/cell
IgG1
107G3B5
n=34
n=44
Example
1
2
3
4

Figure 6

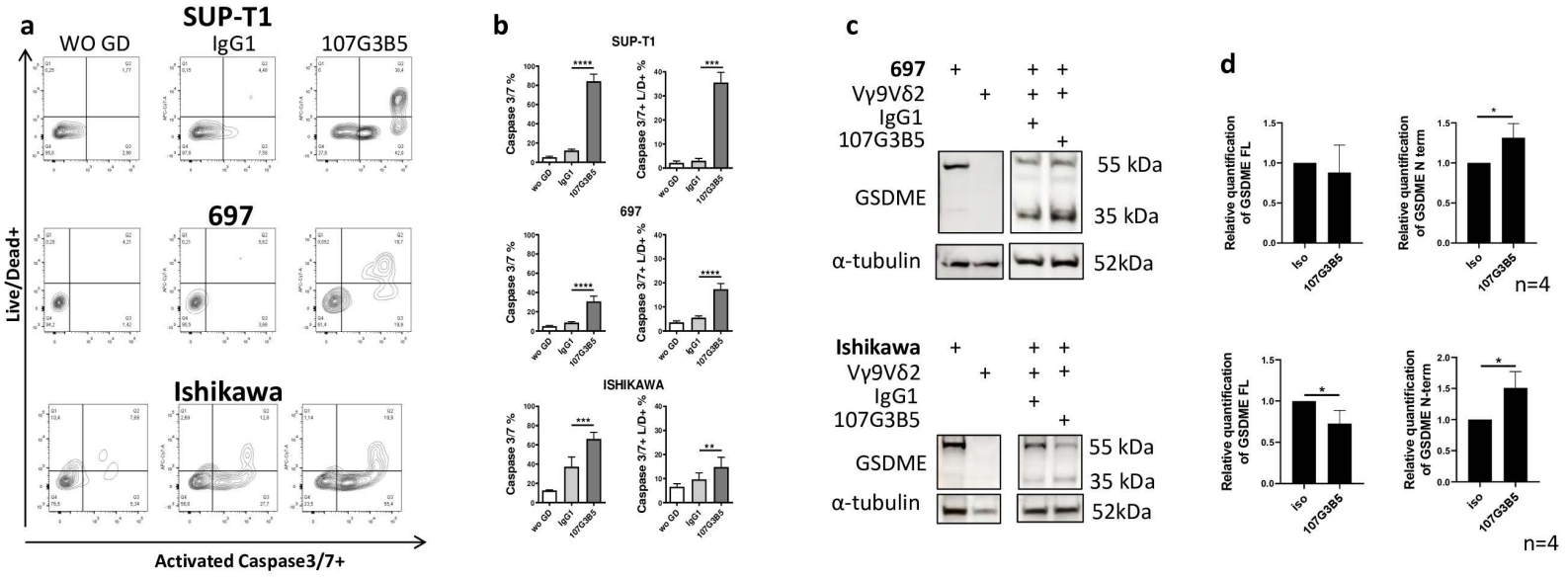
a
SUP-T1
WO GD
IgG1
107G3B5
697
Ishikawa
Live/Dead+
Activated Caspase3/7+
b
SUP-T1
697
ISHIKAWA
Caspase 3/7 %
Caspase 3/7+ L/D+ %
wo GD
IgG1
107G3B5
c
697
Vγ9Vδ2
IgG1
107G3B5
GSDME
α-tubulin
55 kDa
35 kDa
52kDa
Ishikawa
d
Relative quantification of GSDME FL
Relative quantification of GSDME N term
Iso
107G3B5
n=4